

Chemically Self-Consistent Modeling of the Globular Cluster NGC 2808 and its Effects on the Inferred Helium abundance of Multiple Stellar Populations.

EMILY M. BOUDREAU¹, BRIAN C. CHABOYER¹, AMANDA ASH², RENATA EDAES HOH¹, AND GREGORY FEIDEN²

¹*Department of Physics and Astronomy, Dartmouth College, Hanover, NH 03755, USA*

²*Department of Physics and Astronomy, University of North Georgia, Dahlonega, GA 30533, USA*

ABSTRACT

The Helium abundances in the multiple populations which are now known to comprise all closely studied Milky Way globular clusters are often inferred by fitting isochrones generated from stellar evolutionary models to globular cluster photometry. It is therefore important to build stellar models that are chemically self-consistent in terms of their structure, atmosphere, and opacity. In this work we present the first chemically self-consistent stellar models of the Milky Way Globular Cluster NGC 2808 using MARCS model atmospheres, OPLIB high-temperature radiative opacities, and AESOPUS low-temperature radiative opacities. These stellar models were fit to the NGC 2808 photometry using *Fidanka*, a new software tool that was developed optimally fit cluster photometry to isochrones and for population synthesis. *Fidanka* can determine, in a relatively unbiased way, the ideal number of distinct populations which exist within a dataset and then fits isochrones to each population. We achieve this through a combination of Bayesian Gaussian Mixture Modeling and a novel number density estimation algorithm. Using *Fidanka* and F275W-F814W photometry from the Hubble UV Globular Cluster Survey we find that the helium abundance of the second generation of stars in NGC 2808 is higher than the first generation by $15 \pm 3\%$. This is in agreement with previous studies of NGC 2808. **This work, along with previous work by Dotter (2016) focused on NGC 6752 demonstrates that chemically self-consistent models of globular clusters do not significantly alter inferred helium abundances and are therefore unlikely to be worth the significant additional time investment.**

Keywords: Globular Clusters (656), Stellar evolutionary models (2046)

1. INTRODUCTION

Globular clusters (GCs) are among the oldest observable objects in the universe (Peng et al. 2011). They are characterized by high densities with typical half-light radii of ≤ 10 pc (van den Bergh 2010), and typical masses ranging from 10^4 – $10^5 M_{\odot}$ (Brodie & Strader 2006) — though some GCs are significantly larger than these typical values (e.g. ω Cen, Richer et al. 1991). GCs provide a unique way to probe stellar evolution (Baumgardt & Makino 2003), galaxy formation models (Boylan-Kolchin 2018; Kravtsov & Gnedin 2005), and dark matter halo structure (Hudson & Robison 2018).

The traditional view of Globular Clusters was that they consisted of a single stellar population (SSP, in some publications this is referred to as a Simple Stellar Population). This view was supported by spectroscopically uniform heavy element abundances (Carretta et al. 2010; Bastian & Lardo 2018) across most clusters (M54 and ω Cen are notable exceptions, see Marino et al. (2015) for further details), and the lack of evidence for multiple stellar populations (MPs) in past color-magnitude diagrams of GCs (i.e. Sandage 1953; Alcaino 1975). However, over the last 40 years non-trivial star-to-star light-element abundance variations have been observed (i.e. Smith 1987) and, in the last two decades, it has been definitively shown that most if not all Milky Way GCs have MPs (Gratton et al. 2004, 2012; Piotto et al. 2015). The lack of photometric evidence for MPs prior to the 2000, can be attributed to the

54 more narrow color bands available, until very recently, to
55 ground based photometric surveys (Milone et al. 2017).

56 The prevalence of multiple populations in GCs is so
57 distinct that the proposed definitions for what consti-
58 tutes a globular cluster now often center the existence
59 of MPs (e.g. Carretta et al. 2010). Whereas, people have
60 have often tried to categorized objects as GCs through
61 relations between half-light radius, density, and surface
62 brightness profile, in fact many objects which are gener-
63 ally thought of as GCs don't cleanly fit into these cuts
64 (Peebles & Dicke 1968; Brown et al. 1991, 1995; Bekki
65 & Chiba 2002). Consequently, Carretta et al. (2010)
66 proposed a definition of GC based on observed chem-
67 ical inhomogeneities in their stellar populations. The
68 modern understanding of GCs then is not simply one of
69 a dense cluster of stars that may have chemical inho-
70 mogeneities and multiple populations; rather, it is one
71 where those chemical inhomogeneities and multiple pop-
72 ulations themselves are the defining element of a GC.

73 All Milky Way globular clusters studied in detail show
74 populations enriched in He, N, and Na while also be-
75 ing deplete in O and C (Piotto et al. 2015; Bastian &
76 Lardo 2018). **Further, studies of Magellenic Cloud**
77 **massive clusters have shown that these light el-**
78 **ement abundance variations exist in clusters as**
79 **young as ~ 2 Gyr but not in younger clusters**
80 **(Martocchia et al. 2019) while there is also evi-**
81 **dence of nitrogen variability in the ~ 1.5 Gyr old**
82 **cluster NGC 1783 (Cadelano et al. 2022).** These
83 light element abundance patterns also are not strongly
84 correlated with variations in heavy element abundance,
85 resulting in spectroscopically uniform Fe abundances be-
86 tween populations (**though recent work indicates**
87 **that there may be [Fe/H] variations within the**
88 **first population, e.g. Legnardi et al. 2022; Lardo**
89 **et al. 2022)**. Further, high-resolution spectral studies
90 reveal anti-correlations between N-C abundances, Na-O
91 abundances, and potentially Al-Mg (Snedden et al. 1992;
92 Gratton et al. 2012). Typical stellar fusion reactions
93 can deplete core oxygen; however, the observed abun-
94 dances of Na, Al, and Mg cannot be explained by the
95 CNO cycle (Prantzos et al. 2007). Consequently, glob-
96 ular cluster populations must be formed by some novel
97 means.

98 Formation channels for these multiple populations re-
99 main a point of debate among astronomers. Most pro-
100 posed formation channels consist of some older, more
101 massive, population of stars polluting the pristine clus-
102 ter media before a second population forms, now en-
103 riched in heavier elements which they themselves could
104 not have generated (for a detailed review see Gratton
105 et al. 2012). The four primary candidates for these popu-

106 luters are asymptotic giant branch stars (AGBs, Ventura
107 et al. 2001; D'Ercole et al. 2010), fast rotating mas-
108 sive stars (FRMSs, Decressin et al. 2007), super mas-
109 sive stars (SMSs, Denissenkov & Hartwick 2014), and
110 massive interacting binaries (MIBs, de Mink et al. 2009;
111 Bastian & Lardo 2018).

112 Hot hydrogen burning (i.e. proton capture), material
113 transport to the surface, and material ejection into the
114 intra-cluster media are features of each of these models
115 and consequently they can all be made to *qualitatively*
116 agree with the observed elemental abundances. How-
117 ever, none of the standard models can currently account
118 for all specific abundances (Gratton et al. 2012). AGB
119 and FRMS models are the most promising; however,
120 both models have difficulty reproducing severe O deple-
121 tion (Ventura & D'Antona 2009; Decressin et al. 2007).
122 Moreover, AGB and FRMS models require significant
123 mass loss ($\sim 90\%$) between cluster formation and the
124 current epoch — implying that a significant fraction of
125 halo stars formed in GCs (Renzini 2008; D'Ercole et al.
126 2008; Bastian & Lardo 2015).

127 In addition to the light-element anti-correlations ob-
128 served, it is also known that second populations are sig-
129 nificantly enhanced in Helium (Piotto et al. 2007, 2015;
130 Latour et al. 2019). Depending on the cluster, helium
131 mass fractions as high as $Y = 0.4$ have been inferred (e.g.
132 Milone et al. 2015a). However, due to both the relatively
133 high and tight temperature range of partial ionization
134 for He and the efficiency of gravitational settling in core
135 helium burning stars, the initial He abundance of glob-
136 ular cluster stars cannot be observed; consequently, the
137 evidence for enhanced He in GCs originates from com-
138 parison of theoretical stellar isochrones to the observed
139 color-magnitude-diagrams of globular clusters. There-
140 fore, a careful handling of chemistry is essential when
141 modeling with the aim of discriminating between MPs;
142 yet, only a very limited number of GCs have been stud-
143 ied with chemically self-consistent (structure and atmo-
144 sphere) isochrones (e.g. Dotter et al. 2015, NGC 6752).

145 NGC 2808 is the prototype globular cluster to host
146 Multiple Populations. Various studies since 2007 have
147 identified that it may host anywhere from 2-5 stellar
148 populations. These populations have been identified
149 both spectroscopically (i.e. Carretta et al. 2004; Carretta
150 2006; Carretta et al. 2010; Gratton et al. 2011; Carretta
151 2015; Hong et al. 2021) and photometrically (i.e. Piotto
152 et al. 2007, 2015; Milone et al. 2015a, 2017; Pasquato &
153 Milone 2019). Note that recent work (Valle et al. 2022)
154 calls into question the statistical significance of the de-
155 tectations of more than 2 populations in the spectroscopic
156 data. Here we present new, chemically self-consistent
157 modeling of the photometry of the two extreme popula-

158 tions of NGC 2808 identified by Milone et al. (2015a),
 159 populations A and E. **We do not consider popu-**
 160 **lations B, C, or D identified in Milone et al.**
 161 **(2015a) as the purpose of this work is to identi-**
 162 **fy if chemically self-consistent modelling results**
 163 **in a statistically significant deviation in the in-**
 164 **ferred helium abundance when compared to non**
 165 **chemically self-consistent models. Use of the two**
 166 **populations in the NGC 2808 with the highest**
 167 **identified difference between their helium popu-**
 168 **lations is sufficient for to answer this question.** We
 169 use archival photometry from the Hubble UV Globular
 170 Cluster Survey (HUGS) (Piotto et al. 2015; Milone et al.
 171 2017) in the F275W and F814W passbands to charac-
 172 terize multiple populations in NGC 2808 (Milone et al.
 173 2015a,b) (This data is available on MAST Piotto 2018).
 174 Additionally, we present a likelihood analysis of the pho-
 175 tometric data of NGC 2808 to determine the number of
 176 populations present in the cluster.

177 2. CHEMICAL CONSISTENCY

178 There are three primary areas in which must the stel-
 179 lar models must be made chemically consistent: the at-
 180 mospheric boundary conditions, the opacities, and inte-
 181 rior abundances. The interior abundances are relatively
 182 easily handled by adjusting parameters within our stel-
 183 lar evolutionary code. However, the other two areas
 184 are more complicated to bring into consistency. Atmo-
 185 spheric boundary conditions and opacities must both
 186 be calculated with a consistent set of chemical abun-
 187 dances outside of the stellar evolution code. **Nearly all**
 188 **prior efforts at modeling multiple stellar popula-**
 189 **tions in globular clusters have adjusted the abun-**
 190 **dances used in the atmospheric interior models,**
 191 **and in the high temperature opacities, but have**
 192 **not self-consistently modified the corresponding**
 193 **low-temperature opacities and surface boundary**
 194 **conditions, as these are found from stellar atmo-**
 195 **sphere codes, and not the stellar interior codes**
 196 **which are used to create stellar models and**
 197 **isochrones. In this work, as in Dotter (2016),**
 198 **the stellar interior models are chemically self-**
 199 **consistent with the stellar atmosphere models.**
 200 For evolution we use The Dartmouth Stellar Evolution Pro-
 201 gram (DSEP) (Dotter et al. 2008), a well tested 1D
 202 stellar evolution code which has a particular focus on
 203 modelling low mass stars ($\leq 2 M_{\odot}$)

204 2.1. Atmospheric Boundary Conditions

205 Certain assumptions, primarily that the radiation field
 206 is at equilibrium and radiative transport is diffusive
 207 (Salaris & Cassisi 2005), made in stellar structure codes,

208 such as DSEP, are valid when the optical depth of a star
 209 is large. However, in the atmospheres of stars, the num-
 210 ber density of particles drops low enough and the opti-
 211 cal depth consequently becomes small enough that these
 212 assumptions break down, and separate, more physically
 213 motivated, plasma modeling code is required. Generally
 214 structure code will use tabulated atmospheric boundary
 215 conditions generated by these specialized codes, such
 216 as ATLAS9 (Kurucz 1993), PHOENIX (Husser et al.
 217 2013), MARCS (Gustafsson et al. 2008), and MPS-
 218 ATLAS (Kostogryz et al. 2023). Often, as the boundary
 219 conditions are expensive to compute, they are not up-
 220 dated as interior abundances vary.

221 One key element when chemically consistently mod-
 222 eling NGC 2808 modeling is the incorporation of new
 223 atmospheric models with the same elemental abun-
 224 dances as the structure code. We use atmospheres
 225 generated from the MARCS grid of model atmospheres
 226 (Plez 2008). MARCS provides one-dimensional, hydro-
 227 static, plane-parallel and spherical LTE atmospheric
 228 models (Gustafsson et al. 2008). Model atmospheres
 229 are made to match the spectroscopically measured ele-
 230 mental abundances of populations A and E. Moreover,
 231 for each population, atmospheres with various helium
 232 mass fractions are generated. These range from $Y=0.24$
 233 to $Y=0.36$ in steps of 0.03. All atmospheric models are
 234 computed to an optical depth of $\tau = 100$ where their
 235 temperature and pressures serves as boundary condi-
 236 tions for the structure code. In general, enhancing he-
 237 lium in the atmosphere has only a small impact on the
 238 atmospheric temperature profile, while leading to a drop
 239 in the pressure by $\sim 10 - 20\%$.

240 2.2. Opacities

241 In addition to the atmospheric boundary conditions,
 242 both the high and low temperature opacities used by
 243 DSEP must be made chemically consistent. Here we
 244 use OPLIB high temperature opacity tables (Colgan
 245 et al. 2016) retrieved using the TOPS web-interface.
 246 Retrieval of High temperature opacities is done us-
 247 ing pyTOPSScrape, first introduced in Boudreaux &
 248 Chaboyer (2023). Low temperature opacity tables are
 249 retrieved from the Aesopus 2.0 web-interface (Marigo &
 250 Aringer 2009; Marigo et al. 2022). Ideally, these opaci-
 251 ties would be the same used in the atmospheric models.
 252 However, the opacities used in the MARCS models are
 253 not publicly available. As such, we use the opacities pro-
 254 vided by the TOPS and Aesopus 2.0 web-interfaces.

255 3. STELLAR MODELS

256 We use the Dartmouth Stellar Evolution Program
 257 (DSEP, Dotter et al. 2008) to generate stellar models.

Table 1. Population Composition

Element	Pop A	Pop E	Element	Pop A	Pop E
Li	-0.08	—	In	-1.46	—
Be	0.25	—	Sn	-0.22	—
B	1.57	—	Sb	-1.25	—
C	6.87	5.91	Te	-0.08	—
N	6.42	6.69	I	-0.71	—
O	7.87	6.91	Xe	-0.02	—
F	3.43	—	Cs	-1.18	—
Ne	7.12	6.7	Ba	1.05	—
Na	5.11	5.7	La	-0.03	—
Mg	6.86	6.42	Ce	0.45	—
Al	5.21	6.61	Pr	-1.54	—
Si	6.65	6.77	Nd	0.29	—
P	4.28	—	Pm	-99.0	—
S	6.31	5.89	Sm	-1.3	—
Cl	-1.13	4.37	Eu	-0.61	—
Ar	5.59	5.17	Gd	-1.19	—
K	3.9	—	Tb	-1.96	—
Ca	5.21	—	Dy	-1.16	—
Sc	2.02	—	Ho	-1.78	—
Ti	3.82	—	Er	-1.34	—
V	2.8	—	Tm	-2.16	—
Cr	4.51	—	Yb	-1.42	—
Mn	4.3	—	Lu	-2.16	—
Fe	6.37	—	Hf	-1.41	—
Co	3.86	—	Ta	-2.38	—
Ni	5.09	—	W	-1.41	—
Cu	3.06	—	Re	-2.0	—
Zn	2.3	—	Os	-0.86	—
Ga	0.78	—	Ir	-0.88	—
Ge	1.39	—	Pt	-0.64	—
As	0.04	—	Au	-1.34	—
Se	1.08	—	Hg	-1.09	—
Br	0.28	—	Tl	-1.36	—
Kr	0.99	—	Pb	-0.51	—
Rb	0.26	—	Bi	-1.61	—
Sr	0.61	—	Po	-99.0	—
Y	1.08	—	At	-99.0	—
Zr	1.45	—	Rn	-99.0	—
Nb	-0.8	—	Fr	-99.0	—
Mo	-0.38	—	Ra	-99.0	—
Tc	-99.0	—	Ac	-99.0	—
Ru	-0.51	—	Th	-2.2	—
Rh	-1.35	—	Pa	-99.0	—
Pd	-0.69	—	U	-2.8	—

NOTE—Relative Metal composition used where $a(\text{H}) = 12$. Where the relative composition is the the same for both populations A and E it is only listed in the population A column for the sake of visual clarity.

References—Milone et al. (2015a)

DSEP is a one-dimensional stellar evolution code which includes a mixing length model of convection, gravitational settling, and diffusion. Using the solar composition presented in (Grevesse et al. 2007) (GAS07), MARCS model atmospheres, OPLIB high temperature opacities, and AESOPUS 2.0 low temperature opacities we find a solar calibrated mixing length parameter, α_{MLT} , of $\alpha_{MLT} = 1.901$.

We use DSEP to evolve stellar models ranging in mass from 0.3 to 2.0 solar masses from the fully convective pre-main sequence to the tip of the red giant branch. Below $0.7 M_{\odot}$ we evolve a model every $0.03 M_{\odot}$ and above $0.7 M_{\odot}$ we evolve a model every $0.05 M_{\odot}$. We evolve models over a grid of mixing length parameters from $\alpha_{MLT} = 1.0$ to $\alpha_{MLT} = 2.0$ in steps of 0.1. For each mixing length, a grid of models and isochrones were calculated, with chemical compositions consistent with Populations A and E (see Tables 1 and 1) and a range of helium abundances ($Y=0.24, 0.27, 0.30, 0.33, 0.36,$ and 0.39). In total, 144 sets of isochrones, each with a unique composition and mixing length were calculated. Each model is evolved in DSEP with typical numeric tolerances of one part in 10^7 . Each model is allowed a maximum time step of 50 Myr.

For each combination of population, Y , and α_{MLT} we use the isochrone generation code first presented in Dotter (2016) to generate a grid of isochrones. The isochrone generation code identified equivalent evolutionary points (EEPs) over a series of masses and interpolates between them. The grid of isochrones generated for this work is available as a digital supplement to this paper [10.5281/zenodo.10631439](https://doi.org/10.5281/zenodo.10631439). Given the complexity of the parameter space when fitting multiple populations along with the recent warnings in the literature regarding overfitting datasets (e.g. Valle et al. 2022) we want to develop a more objective way of fitting isochrones to photometry than if we were to mark median ridge line positions by hand.

4. FIDANKA

When fitting isochrones to the clusters with multiple populations we have four main criteria for any method

- The method must be robust enough to work along the entire main sequence, turn off, and much of the subgiant and red giant branch.
- Any method should consider photometric uncertainty in the fitting process.

Table 2. Population Abundance Ratios

Population	[Fe/H]	[α /Fe]	[C/Fe]	[N/Fe]	[O/Fe]	[r/Fe]	[s/Fe]	C/O	X	Y	Z
A	-1.13	0.32	-0.43	-0.28	0.31	-1.13	-1.13	0.10	0.7285	0.2700	0.00154
E	-1.13	-0.11	-1.39	-0.02	-0.66	-1.13	-1.13	0.10	0.7594	0.240	0.00063

NOTE—Abundance Ratios for populations A and E in NGC 2808.

References—Milone et al. (2015a)

- The method should be model independent, weighting any n number of populations equally.
- The method should be automated and require minimal intervention from the user.

We do not believe that any currently available software is a match for our use case. Therefore, we elect to develop our own software suite, **Fidanka**. **Fidanka** is a python package designed to automate much of the process of measuring fiducial lines in CMDs, adhering to the four criteria we lay out above. Primary features of **Fidanka** may be separated into three categories: fiducial line measurement, stellar population synthesis, and isochrone optimization/fitting. Additionally, there are utility functions that are detailed in the **Fidanka** documentation.

4.1. Fiducial Line Measurement

Fidanka takes an iterative approach to measuring fiducial lines, the first step of which is to make a “guess” as to the fiducial line. This initial guess is calculated by splitting the CMD into magnitude bins, with uniform numbers of stars per bin (so that bins cover a small magnitude range over densely populated regions of the CMD while covering a much larger magnitude range in sparsely populated regions of the CMD, such as the RGB). A unimodal Gaussian distribution is then fit to the color distribution of each bin, and the resulting mean color is used as the initial fiducial line guess. This rough fiducial line will approximately trace the area of highest density. The initial guess will be used to verticalize the CMD so that further algorithms can work in 1-D magnitude bins without worrying about weighting issues caused by varying projections of the evolutionary sequence onto the magnitude axis. Verticalization is performed taking the difference between the guess fiducial line and the color of each star in the CMD.

If **Fidanka** were to simply apply the same algorithm to the verticalized CMD then the resulting fiducial line would likely be a re-extraction of the initial fiducial line guess. To avoid this, we take a more robust, num-

ber density based approach, which considers the distribution of stars in both color and magnitude space simultaneously. For each star in the CMD we first use an **introslect** partitioning algorithm to select the 50 nearest stars in F814W vs. F275W-F814W space. To account for the case where the star is at an extreme edge of the CMD, those 50 stars include the star itself (such that we really select 49 stars + 1). We use **qhull**¹ (Barber et al. 1996) to calculate the convex hull of those 50 points. The number density at each star then is defined as $50/A_{hull}$, where A_{hull} is the area of the convex hull. Because we use a fixed number of points per star, and a partitioning algorithm as opposed to a sorting algorithm, this method scales like $\mathcal{O}(n)$, where n is the number of stars in the CMD. This method also intrinsically weights the density of each star equally as the counting statistics per bin are uniform. We are left with a CMD where each star has a defined number density (Figure 1).

Fidanka can now exploit this density map to fit a better fiducial line to the data, as the density map is far more robust to outliers. There are multiple algorithms we implement to fit the fiducial line to the color-density profile in each magnitude bin (Figure 2); they are explained in more detail in the **Fidanka** documentation. However, of most relevance here is the Bayesian Gaussian Mixture Modeling (BGMM) method. BGMM is a clustering algorithm which, for some fixed number of n -dimensional Gaussian distributions, K , determines the mean, covariance, and mixing probability (somewhat analogous to amplitude) of each k^{th} distribution, such that the local lower bound of the likelihood of each star belonging strongly to a single distribution is maximized. Maximization is performed using the Dirichlet process, which is a non-parametric Bayesian method of determining the number of Gaussian distributions, K , which best fit the data (Ferguson 1973; Pedregosa et al. 2011). Use of the Dirichlet process allows for dynamic variation in the number of inferred populations from

¹ <https://www.qhull.com>

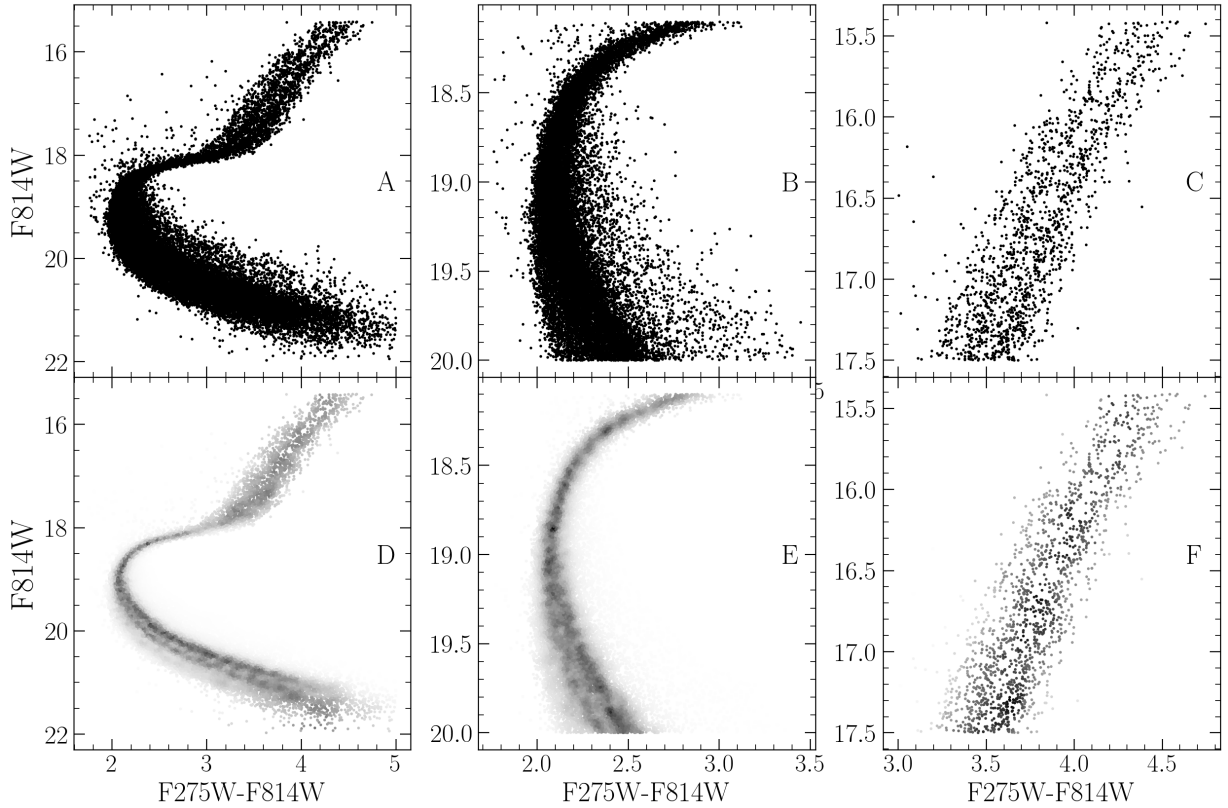


Figure 1. Figures in the top row are the raw CMD, while figures in the bottom row are colored by the density map. Density map demo showing density estimate over different parts of the evolutionary sequence. The left panel shows the density map over the entire evolutionary sequence, while the middle panel shows the density map over the main sequence and the right most panel shows the density map over the RGB.

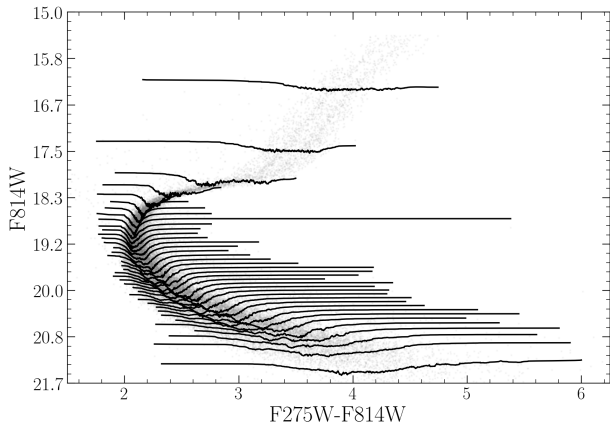


Figure 2. CMD where point brightness is determined by local density. Lines show the density-color profile in each magnitude bin. In this figure adaptive binning targeted 1000 stars per bin

382 magnitude bin to magnitude bin. Specifically, popula-
 383 tions are clearly visually separated from the lower main
 384 sequence through the turn off; however, at the turn off
 385 and throughout much of the subgiant branch, the two
 386 visible populations overlap due to their extremely simi-

387 lar ages (i.e. [Jordán et al. 2002](#)). The Dirichlet process
 388 allows for the BGMM method to infer a single popula-
 389 tion in these regions, while inferring two populations in
 390 regions where they are clearly separated. More gener-
 391 ally, the use of the Dirichlet process removes the need
 392 for a prior on the exact number of populations to fit.
 393 Rather, the user specifies a upper bound on the num-
 394 ber of populations within the cluster. An example bin
 395 ($F814W = 20.6$) is shown in [Figure 3](#).

396 **Fidanka** 's BGMM method first breaks down the ver-
 397 ticalized CMD into magnitude bins with uniform num-
 398 bers of stars per bin (here we adopt 250). Any stars
 399 left over are placed into the final bin. For each bin a
 400 BGMM model with a maximum of 5 populations is fit
 401 to the color density profile. The number of populations
 402 is then inferred from the weighting parameter (the mix-
 403 ing probability) of each population. If the weighting pa-
 404 rameter of any k^{th} components less than 0.05, then that
 405 component is considered to be spurious and removed.
 406 Additionally, if the number of populations in the bin
 407 above and the bin below are the same, then the num-
 408 ber of populations in the current bin is forced to be the
 409 same as the number of populations in the bin above. Fi-

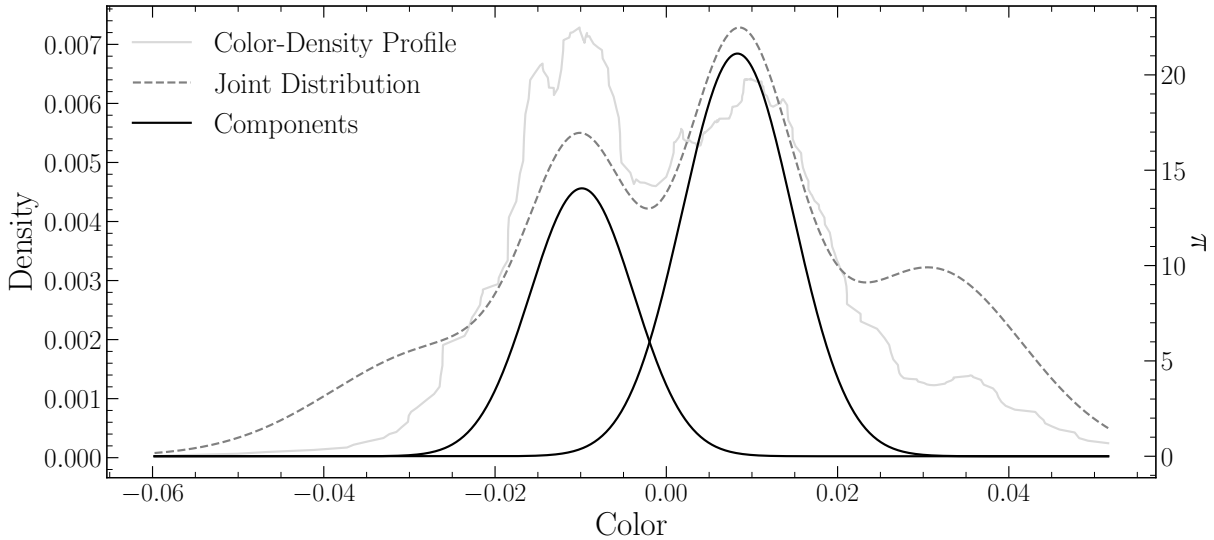


Figure 3. Example of BGMM fit to a magnitude bin. The grey line shows the underlying color-density profile, while the black dashed-line shows the joint distribution of each BGMM component. The solid black lines show the two selected components.

nally, the initial guess fiducial line is added back to the BGMM inferred line. Figure 4 shows the resulting fiducial line(s) in each magnitude bin for both a verticalized CMD and a non verticalized CMD. In contrast to other work in the literature where evidence for up to 5 distinct populations has been found; we only find evidence for two stellar populations.

This method of fiducial line extraction effectively discriminated between multiple populations along the main sequence and RGB of a cluster, while simultaneously allowing for the presence of a single population along the MSTO and subgiant branch.

We can adapt this density map based BGMM method to consider photometric uncertainties by adopting a simple Monte Carlo approach. Instead of measuring the fiducial line(s) a single time, *Fidanka* can measure the fiducial line(s) many times, resampling the data with replacement each time. For each resampling *Fidanka* adds a random offset to each filter based on the photometric uncertainties of each star. From these n measurements the mean fiducial line for each sequence can be identified along with upper and lower bound confidence intervals in each magnitude bin.

4.2. Stellar Population Synthesis

While not extensively used in this paper *Fidanka* can, in addition to measuring fiducial lines, perform stellar population synthesis. *Fidanka*'s population synthesis module can generate synthetic stellar population from a set of MIST formatted isochrones. This is of primary importance for binary population modeling. The module is also used to generate synthetic CMDs for the purpose

of testing the fiducial line extraction algorithms against priors.

Fidanka uses MIST formatted isochrones (Dotter 2016) as input along with distance modulus, B-V color excess, binary mass fraction, and bolometric corrections. An arbitrarily large number of isochrones may be used to define an arbitrary number of populations. Synthetic stars are samples from each isochrone based on a definable probability (for example it is believed that $\sim 90\%$ of stars in globular clusters are younger population (e.g. Suntzeff & Kraft 1996; Carretta 2013)). Based on the metallicity, μ , and E(B-V) of each isochrone, bolometric corrections are taken from bolometric correction tables. Where bolometric correction tables do not include exact metallicities or extinctions a linear interpolation is performed between the two bounding values.

4.3. Isochrone Optimization

The optimization routines in *Fidanka* will find the best fit distance modulus, B-V color excess, and binary number fraction for a given set of isochrones. If a single isochrone is provided then the optimization is done by minimizing the χ^2 of the perpendicular distances between an isochrone and a fiducial line. If multiple isochrones are provided then those isochrones are first used to run stellar population synthesis and generate a synthetic CMD. The optimization is then done by minimizing the χ^2 of both the perpendicular distances between and widths of the observed fiducial line and the fiducial line of the synthetic CMD.

4.4. *Fidanka* Testing

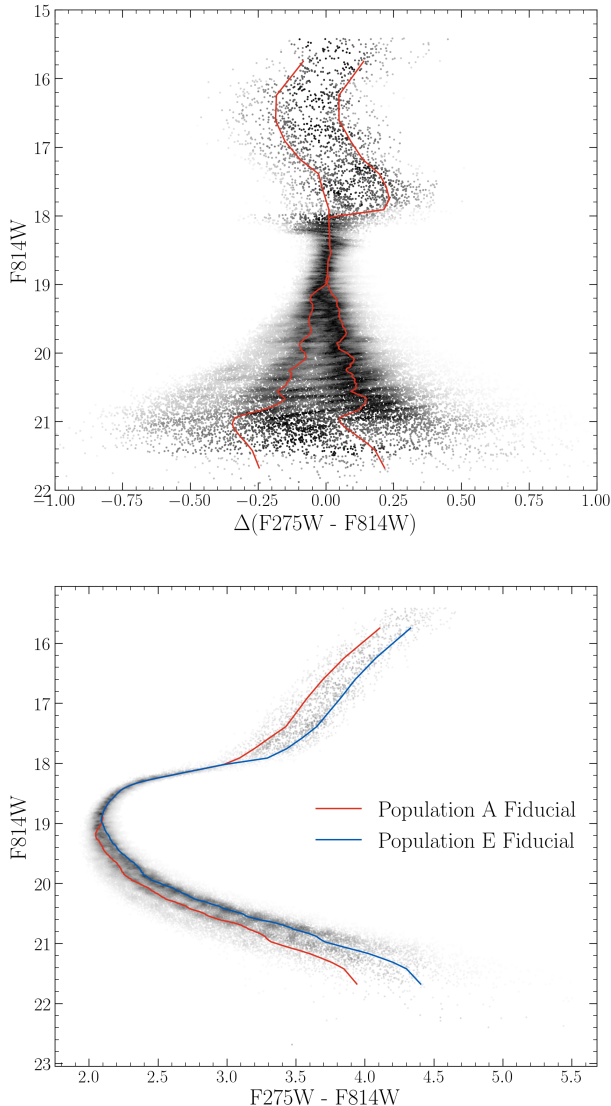


Figure 4. Verticalized CMD (where the color of each data point is subtracted from the color of the fiducial line at that magnitude) where point brightness is determined by density (top). CMD where point brightness is determined by density, calculated fiducial lines are shown (bottom). The data used is from the Hubble Space Telescope UV Legacy Survey of Galactic Globular Clusters.

471 In order to validate *fidanka* we have run an series of
 472 injection recovery tests using *Fidanka*'s population syn-
 473 thesis routines to build various synthetic populations
 474 and *Fidanka*'s fiducial measurement routines to recover
 475 these populations. Each population was generated using
 476 the initial mass function given in (Milone et al. 2012)
 477 for the redmost population ($\alpha = -1.2$). Further, every
 478 population was given a binary population fraction of
 479 10%, distance uniformly sampled between 5000pc and
 480 15000pc, and a B-V color excess uniformly sampled be-
 481 tween 0 and 0.1. Finally, each synthetic population was

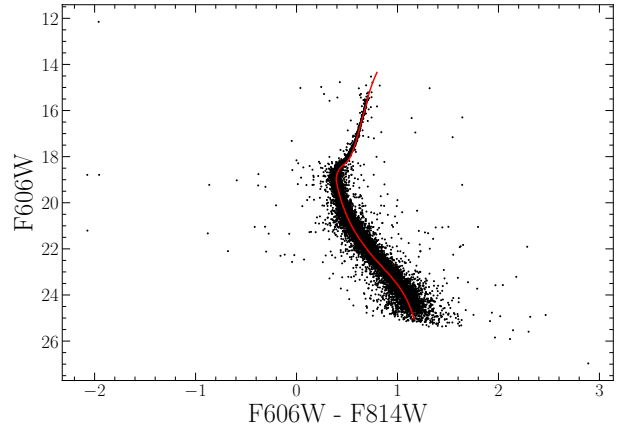


Figure 5. Synthetic population generated by *fidanka* at 10000pc with $E(B-V) = 0$, and an age of 12 Gyr along with the best fitting isochrone. The best fit parameters are derived to be $\mu = 15.13$, $E(B-V)=0.001$, and an age of 12.33 Gyr.

482 generated using a fixed age uniformly sampled between
 483 7 Gyr and 14 Gyr. An example synthetic population
 484 along with its associated best fit isochrone are shown in
 485 Figure 5.

486 For each trial we use *Fidanka* to measure the fiducial
 487 line and then optimize that fiducial line against the origi-
 488 nating isochrone to estimate distance modulus, age, and
 489 color B-V excess. Figure 6 is built from 1000 **Monte-**
 490 **Carlo** trials and shows the mean and width of the per-
 491 cent error distributions for μ , A_v , and age. In general
 492 *Fidanka* is able to recover distance moduli effectively
 493 with age and $E(B-V)$ recovery falling in line with other
 494 literature that does not consider the CMD outside of the
 495 main sequence, main sequence turn off, sub giant, and
 496 red giant branches; specifically, it should be noted that
 497 *Fidanka* is not setup to model the horizontal branch.

5. ISOCHRONE FITTING

498
 499 We fit pairs of isochrones to the HUGS data for NGC
 500 2808 using *Fidanka*, as described in §4. Two isochrones,
 501 one for Population A and one for Population E are fit si-
 502 multaneously. These isochrones are constrained to have
 503 distance modulus, μ , and color excess, $E(B-V)$ which
 504 agree to within 0.5% and an ages which agree to within
 505 1%. Moreover, we constrain the mixing length, α_{ML} ,
 506 for any two isochrones in a set to be within 0.5 of one
 507 and other. For every isochrone in the set of combina-
 508 tion of which fulfilling these constraints μ , $E(B-V)$,
 509 Age_A , and Age_B are optimized to reduce the χ^2 distance
 510 ($\chi^2 = \sum \sqrt{\Delta color^2 + \Delta mag^2}$) between the fiducial lines
 511 and the isochrones. Because we fit fiducial lines directly,
 512 we do not need to consider the binary population frac-
 513 tion, f_{bin} , as a free parameter.

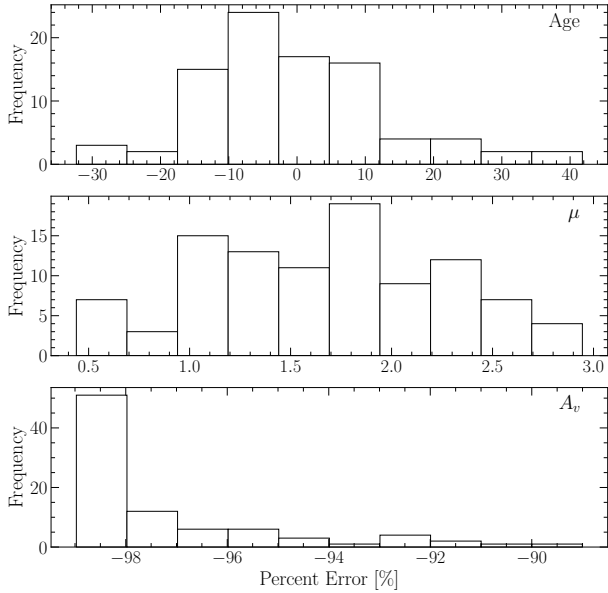


Figure 6. Percent Error distribution for each of the three deriver parameters. Note that these values will be sensitive to the magnitude uncertainties of the photometry. Here we made use of the ACS artificial star tests to estimate the uncertainties.

514 The best fit isochrones are shown in Figure 7 and op-
 515 timized parameters for these are presented in Table 1.
 516 **The initial guess for the age of these populations**
 517 **was locked to 12 Gyr and the initial Extinction**
 518 **was locked to 0.5 mag. The initial guess for the**
 519 **distance modulus was determined at run time**
 520 **using a dynamic time warping algorithm to best**
 521 **align the morphologies of the fiducial line with**
 522 **the target isochrone. This algorithm is explained**
 523 **in more detail in the Fidanka documentation un-**
 524 **der the function called guess_mu We find helium**
 525 **mass fractions that are consistent with those identified**
 526 **in past literature (e.g. Milone et al. 2015a). Note that**
 527 **our helium mass fraction grid has a spacing of 0.03 be-**
 528 **tween grid points and we are therefore unable to resolve**
 529 **between certain proposed helium mass fractions for the**
 530 **younger sequence (for example between 0.37 and 0.39).**
 531 **We also note that the best fit mixing length pa-**
 532 **rameter which we derive for populations A and**
 533 **E do not agree within their uncertainties. This is**
 534 **not suprising as the much high mean molecular**
 535 **mass of population E — when compared to pop-**
 536 **ulation A, due to population E’s larger helium**
 537 **mass fraction — will result in a steaper adiabatic**
 538 **temperature gradient**

539 Past literature (e.g. Milone et al. 2015a, 2018) have
 540 found helium mass fraction variation from the low red-
 541 most to bluemost populations of ~ 0.12 . Here we find a

542 helium mass fraction variation of 0.15 which, given the
 543 spacing of the helium grid we use *is consistent with these*
 544 *past results.*

545 5.1. The Number of Populations in NGC 2808

546 In order to estimate the number of populations which
 547 ideally fit the NGC 2808 F275W-F814W photometry
 548 without overfitting the data we make use of silhouette
 549 analysis (Rousseeuw 1987, and in a similar manner to
 550 how Valle et al. (2022) preform their analysis of spectro-
 551 scopic data). We find the average silhouette score for all
 552 tagged clusters identified using BGMM in all magnitude
 553 bins over the CMD using the standar python module
 554 sklearn. Figure 8 shows the silhouette analysis results
 555 and that two populations fit the photometry most ideally.
 556 This is in line with what our BGMM model predicts
 557 for the majority of the the CMD.

558 **While we make use a purley CMD based ap-**
 559 **proach in this work, other literature has made**
 560 **use of Chromosome Maps. These consist of im-**
 561 **PLICITLY verticalized pseudo colors. In the chro-**
 562 **mosome map for NGC 2808 there may be evi-**
 563 **dence for more than two populations; however,**
 564 **the process of transforming magnitude measure-**
 565 **ments into chromosome space results in dramati-**
 566 **cally increased uncertainties for each star. We**
 567 **find a mean fractional uncertantie for chromo-**
 568 **some parameters of ≈ 1 when starting with mag-**
 569 **nitude measurements having a mean best-case**
 570 **(i.e. uncertainty assumed to only be due to Pois-**
 571 **son statistics) fractional uncertainty of ≈ 0.0005 .**
 572 **Because of how Fidanka operates, i.e. resampling**
 573 **a probabily distribution for each star in order to**
 574 **identify clusters, we are unable to make statisti-**
 575 **cally meaningful statements from the chromo-**
 576 **some map**

577 5.2. ACS-HUGS Photometric Zero Point Offset

578 The Hubble legacy archive photometry used in this
 579 work is calibrated to the Vega magnitude system. How-
 580 ever, we have found that the photometry has a system-
 581 atic offset of ~ 0.026 magnitudes in the F814W band
 582 when compared to the same stars in the ACS survey
 583 (Figure 9). The exact cause of this offset is unknown,
 584 but it is likely due to a difference in the photometric
 585 zero point between the two surveys. A full correction
 586 of this offset would require a careful re-reduction of the
 587 HUGS photometry, which is beyond the scope of this
 588 work. We instead recognize a 0.02 inherent uncertainty
 589 in the inferred magnitude of any fit when comparing to
 590 the ACS survey. This uncertainty is small when com-

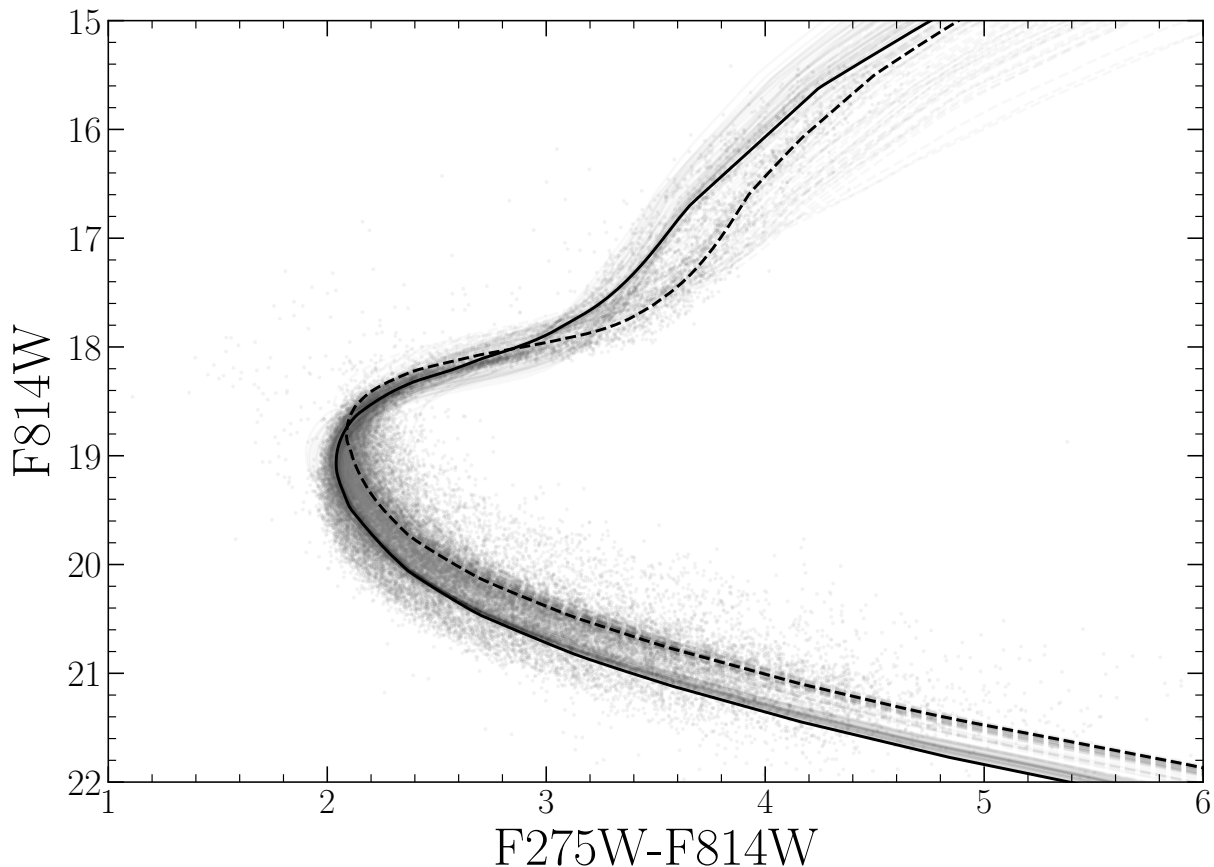


Figure 7. Best fit isochrone results for NGC 2808. The best fit population A and E models are shown as black lines. The following 50 best fit models are presented as grey lines. The solid black line is fit to population A, while the dashed black line is fit to population E.

Population	Age [Gyr]	Distance Modulus	Extinction [mag]	Y	α_{ML}	χ^2_ν
A	$12.996^{+0.87}_{-0.64}$	15.021	0.54	0.24	2.050	0.021
E	$13.061^{+0.86}_{-0.69}$	15.007	0.537	0.39	1.600	0.033

Table 1. Best fit parameters derived from fitting isochrones to the fiducial lines derived from the NCG 2808 photometry. The one sigma uncertainty reported on population age were determined from the 16th and 84th percentiles of the distribution of best fit isochrones ages.

591 pared to the uncertainty in the distance modulus and
592 should not affect the conclusion of this paper.

593 The observed photometric offset between ACS and
594 HUGS reductions introduces a systematic uncertainty
595 when comparing parameters derived from isochrone fits
596 to ACS data vs those fit to HUGS data. Specifically, this
597 offset introduces a $\sim 2Gyr$ uncertainty when compar-
598 ing ages between ACS and HUGS. Moreover, for two
599 isochrone of the same age, only separated by helium
600 mass fraction, a shift of the main sequence turn off of
601 is also expected. Figure 10 shows this shift. Note a
602 change in the helium mass fraction of a model by 0.03
603 results in an approximate 0.08 magnitude shift to the

604 main sequence turn off location. This means that the
605 mean 0.026 magnitude offset we find in between ACS
606 and HUGS data corresponds to an additional approxi-
607 mate 0.01 uncertainty in the derived helium mass frac-
608 tion when comparing between these two datasets.

609 6. CONCLUSION

610 Here we have preformed the first chemically self-
611 consistent modeling of the Milky Way Globular Cluster
612 NGC 2808. We find that, updated atmospheric bound-
613 ary conditions and opacity tables do not have a signif-
614 icant effect on the inferred helium abundances of mul-
615 tiple populations. Specifically, we find that population

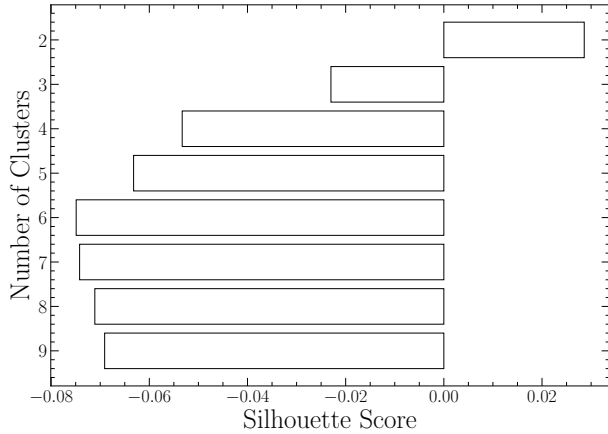


Figure 8. Silhouette analysis for NGC 2808 F275W-F814W photometry. The Silhouette scores are an average of score for each magnitude bin. Positive scores indicate that the clustering algorithm produced well distinguished clusters while negative scores indicate clusters which are not well distinguished.

616 has a helium mass fraction of 0.24, while population E

617 has a helium mass fraction of 0.39. Additionally, we
 618 find that the ages of these two populations agree within
 619 uncertainties. We only find evidence for two distinct
 620 stellar populations, which is in agreement with recent
 621 work studying the number of populations in NGC 2808
 622 spectroscopic data.

623 We introduce a new software suite for globular cluster
 624 science, *Fidanka*, which has been released under a per-
 625 missive open source license. *Fidanka* aims to provide a
 626 statistically robust set of tools for estimating the param-
 627 eters of multiple populations within globular clusters.

628 This work has made use of the NASA astrophysical data
 629 system (ADS). We would like to thank Elisabeth New-
 630 ton and Aaron Dotter for their support and for useful
 631 discussion related to the topic of this paper. Addition-
 632 ally, we would like to thank Kara Fagerstrom, Aylin
 633 Garcia Soto, and Keighley Rockcliffe for their useful
 634 discussion related to in this work. We acknowledge the
 635 support of a NASA grant (No. 80NSSC18K0634).

REFERENCES

- 636 Alcaïno, G. 1975, *A&AS*, 21, 15
- 637 Barber, C. B., Dobkin, D. P., & Huhdanpaa, H. 1996, *ACM*
 638 *Transactions on Mathematical Software (TOMS)*, 22, 469
- 639 Bastian, N., & Lardo, C. 2015, *MNRAS*, 453, 357,
 640 doi: [10.1093/mnras/stv1661](https://doi.org/10.1093/mnras/stv1661)
- 641 Bastian, N., & Lardo, C. 2018, *Annual Review of*
 642 *Astronomy and Astrophysics*, 56, 83
- 643 Baumgardt, H., & Makino, J. 2003, *MNRAS*, 340, 227,
 644 doi: [10.1046/j.1365-8711.2003.06286.x](https://doi.org/10.1046/j.1365-8711.2003.06286.x)
- 645 Bekki, K., & Chiba, M. 2002, *The Astrophysical Journal*,
 646 566, 245, doi: [10.1086/337984](https://doi.org/10.1086/337984)
- 647 Boudreaux, E. M., & Chaboyer, B. C. 2023, *ApJ*, 944, 129,
 648 doi: [10.3847/1538-4357/acb685](https://doi.org/10.3847/1538-4357/acb685)
- 649 Boylan-Kolchin, M. 2018, *MNRAS*, 479, 1423,
 650 doi: [10.1093/mnras/sty1490](https://doi.org/10.1093/mnras/sty1490)
- 651 Brodie, J. P., & Strader, J. 2006, *Annu. Rev. Astron.*
 652 *Astrophys.*, 44, 193
- 653 Brown, J. H., Burkert, A., & Truran, J. W. 1991, *ApJ*, 376,
 654 115, doi: [10.1086/170260](https://doi.org/10.1086/170260)
- 655 —. 1995, *ApJ*, 440, 666, doi: [10.1086/175304](https://doi.org/10.1086/175304)
- 656 Cadelano, M., Dalessandro, E., Salaris, M., et al. 2022,
 657 *ApJL*, 924, L2, doi: [10.3847/2041-8213/ac424a](https://doi.org/10.3847/2041-8213/ac424a)
- 658 Carretta, E. 2006, *AJ*, 131, 1766, doi: [10.1086/499565](https://doi.org/10.1086/499565)
- 659 —. 2013, *A&A*, 557, A128,
 660 doi: [10.1051/0004-6361/201322103](https://doi.org/10.1051/0004-6361/201322103)
- 661 —. 2015, *ApJ*, 810, 148, doi: [10.1088/0004-637X/810/2/148](https://doi.org/10.1088/0004-637X/810/2/148)
- 662 Carretta, E., Bragaglia, A., & Cacciari, C. 2004, *ApJL*,
 663 610, L25, doi: [10.1086/423034](https://doi.org/10.1086/423034)
- 664 Carretta, E., Bragaglia, A., Gratton, R. G., et al. 2010,
 665 *Astronomy & Astrophysics*, 516, A55
- 666 Colgan, J., Kilcrease, D. P., Magee, N. H., et al. 2016, in
 667 *APS Meeting Abstracts*, Vol. 2016, APS Division of
 668 *Atomic, Molecular and Optical Physics Meeting*
 669 *Abstracts*, D1.008
- 670 de Mink, S. E., Pols, O. R., Langer, N., & Izzard, R. G.
 671 2009, *A&A*, 507, L1, doi: [10.1051/0004-6361/200913205](https://doi.org/10.1051/0004-6361/200913205)
- 672 Decressin, T., Meynet, G., Charbonnel, C., Prantzos, N., &
 673 Ekström, S. 2007, *A&A*, 464, 1029,
 674 doi: [10.1051/0004-6361:20066013](https://doi.org/10.1051/0004-6361:20066013)
- 675 Denissenkov, P. A., & Hartwick, F. D. A. 2014, *MNRAS*,
 676 437, L21, doi: [10.1093/mnras/slt133](https://doi.org/10.1093/mnras/slt133)
- 677 D’Ercole, A., D’Antona, F., Ventura, P., Vesperini, E., &
 678 McMillan, S. L. W. 2010, *MNRAS*, 407, 854,
 679 doi: [10.1111/j.1365-2966.2010.16996.x](https://doi.org/10.1111/j.1365-2966.2010.16996.x)
- 680 D’Ercole, A., Vesperini, E., D’Antona, F., McMillan, S.
 681 L. W., & Recchi, S. 2008, *MNRAS*, 391, 825,
 682 doi: [10.1111/j.1365-2966.2008.13915.x](https://doi.org/10.1111/j.1365-2966.2008.13915.x)
- 683 Dotter, A. 2016, *ApJS*, 222, 8,
 684 doi: [10.3847/0067-0049/222/1/8](https://doi.org/10.3847/0067-0049/222/1/8)
- 685 Dotter, A., Chaboyer, B., Jevremović, D., et al. 2008, *The*
 686 *Astrophysical Journal Supplement Series*, 178, 89
- 687 Dotter, A., Ferguson, J. W., Conroy, C., et al. 2015,
 688 *MNRAS*, 446, 1641, doi: [10.1093/mnras/stu2170](https://doi.org/10.1093/mnras/stu2170)

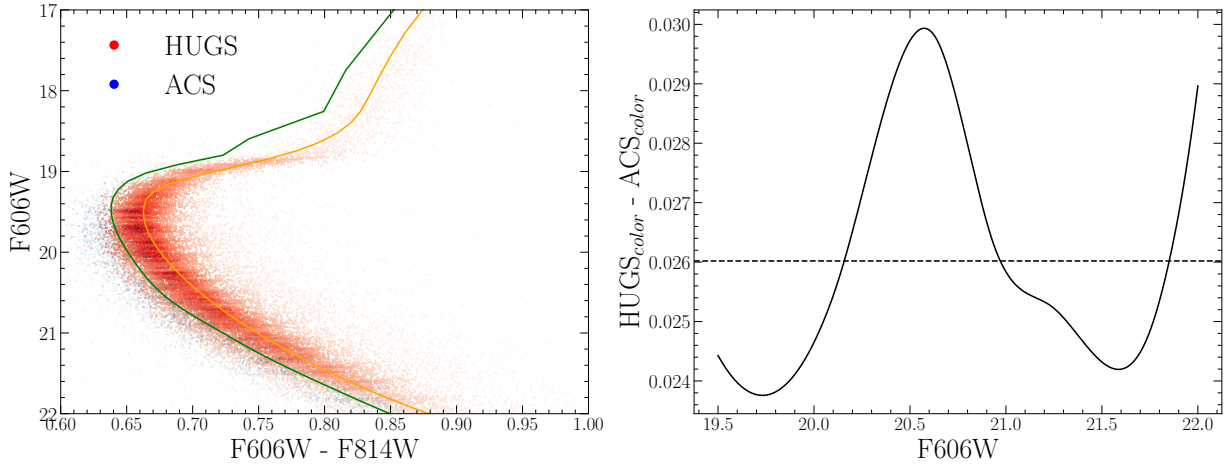


Figure 9. (left) CMD showing the photometric offset between the ACS and HUGS data for NGC 2808. CMDs have been randomly subsampled and colored by point density for clarity. (right) Mean difference between the color of the HUGS and ACS fiducial lines at the same magnitude. Note that the ACS data is systematically bluer than the HUGS data.

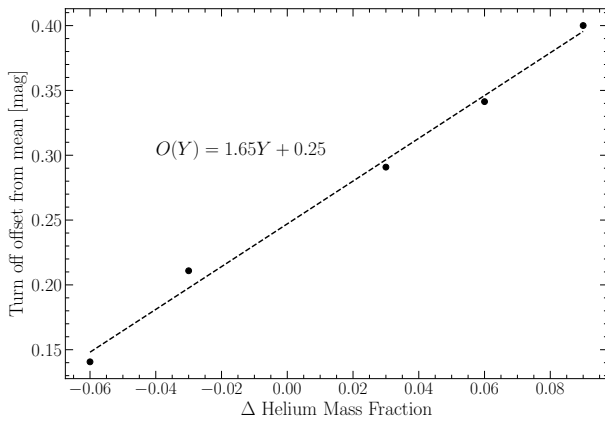


Figure 10. Main sequence turn off magnitude offset from a gauge helium mass fraction ($Y=0.30$ chosen). All main sequence turn off locations are measured at 12.3 Gyr

689 Ferguson, T. S. 1973, *The annals of statistics*, 209
 690 Gratton, R., Sneden, C., & Carretta, E. 2004, *ARA&A*, 42,
 691 385, doi: [10.1146/annurev.astro.42.053102.133945](https://doi.org/10.1146/annurev.astro.42.053102.133945)
 692 Gratton, R. G., Carretta, E., & Bragaglia, A. 2012,
 693 *Astronomy and Astrophysics Reviews*, 20, 50,
 694 doi: [10.1007/s00159-012-0050-3](https://doi.org/10.1007/s00159-012-0050-3)
 695 Gratton, R. G., Lucatello, S., Carretta, E., et al. 2011,
 696 *A&A*, 534, A123, doi: [10.1051/0004-6361/201117690](https://doi.org/10.1051/0004-6361/201117690)
 697 Grevesse, N., Asplund, M., & Sauval, A. J. 2007, *SSRv*,
 698 130, 105, doi: [10.1007/s11214-007-9173-7](https://doi.org/10.1007/s11214-007-9173-7)
 699 Gustafsson, B., Edvardsson, B., Eriksson, K., et al. 2008,
 700 *A&A*, 486, 951, doi: [10.1051/0004-6361:200809724](https://doi.org/10.1051/0004-6361:200809724)
 701 Hong, S., Lim, D., Chung, C., et al. 2021, *AJ*, 162, 130,
 702 doi: [10.3847/1538-3881/ac0ce6](https://doi.org/10.3847/1538-3881/ac0ce6)
 703 Hudson, M. J., & Robison, B. 2018, *Monthly Notices of the*
 704 *Royal Astronomical Society*, 477, 3869,
 705 doi: [10.1093/mnras/sty844](https://doi.org/10.1093/mnras/sty844)

706 Husser, T. O., Wende-von Berg, S., Dreizler, S., et al. 2013,
 707 *A&A*, 553, A6, doi: [10.1051/0004-6361/201219058](https://doi.org/10.1051/0004-6361/201219058)
 708 Jordán, A., Côté, P., West, M. J., & Marzke, R. O. 2002,
 709 *ApJL*, 576, L113, doi: [10.1086/343759](https://doi.org/10.1086/343759)
 710 Kostogryz, N., Shapiro, A. I., Witzke, V., et al. 2023,
 711 *Research Notes of the AAS*, 7, 39,
 712 doi: [10.3847/2515-5172/acc180](https://doi.org/10.3847/2515-5172/acc180)
 713 Kravtsov, A. V., & Gnedin, O. Y. 2005, *The Astrophysical*
 714 *Journal*, 623, 650
 715 Kurucz, R.-L. 1993, *Kurucz CD-Rom*, 13
 716 Lardo, C., Salaris, M., Cassisi, S., & Bastian, N. 2022,
 717 *A&A*, 662, A117, doi: [10.1051/0004-6361/202243843](https://doi.org/10.1051/0004-6361/202243843)
 718 Latour, M., Husser, T. O., Giesers, B., et al. 2019, *A&A*,
 719 631, A14, doi: [10.1051/0004-6361/201936242](https://doi.org/10.1051/0004-6361/201936242)
 720 Legnardi, M. V., Milone, A. P., Armillotta, L., et al. 2022,
 721 *MNRAS*, 513, 735, doi: [10.1093/mnras/stac734](https://doi.org/10.1093/mnras/stac734)
 722 Marigo, P., & Aringer, B. 2009, *A&A*, 508, 1539,
 723 doi: [10.1051/0004-6361/200912598](https://doi.org/10.1051/0004-6361/200912598)
 724 Marigo, P., Aringer, B., Girardi, L., & Bressan, A. 2022,
 725 *ApJ*, 940, 129, doi: [10.3847/1538-4357/ac9b40](https://doi.org/10.3847/1538-4357/ac9b40)
 726 Marino, A. F., Milone, A. P., Karakas, A. I., et al. 2015,
 727 *Monthly Notices of the Royal Astronomical Society*, 450,
 728 815, doi: [10.1093/mnras/stv420](https://doi.org/10.1093/mnras/stv420)
 729 Martocchia, S., Dalessandro, E., Lardo, C., et al. 2019,
 730 *Monthly Notices of the Royal Astronomical Society*, 487,
 731 5324, doi: [10.1093/mnras/stz1596](https://doi.org/10.1093/mnras/stz1596)
 732 Milone, A. P., Piotto, G., Bedin, L. R., et al. 2012, *ApJ*,
 733 744, 58, doi: [10.1088/0004-637X/744/1/58](https://doi.org/10.1088/0004-637X/744/1/58)
 734 Milone, A. P., Marino, A. F., Piotto, G., et al. 2015a, *ApJ*,
 735 808, 51, doi: [10.1088/0004-637X/808/1/51](https://doi.org/10.1088/0004-637X/808/1/51)
 736 —. 2015b, *MNRAS*, 447, 927, doi: [10.1093/mnras/stu2446](https://doi.org/10.1093/mnras/stu2446)
 737 Milone, A. P., Piotto, G., Renzini, A., et al. 2017, *MNRAS*,
 738 464, 3636, doi: [10.1093/mnras/stw2531](https://doi.org/10.1093/mnras/stw2531)

- 739 Milone, A. P., Marino, A. F., Renzini, A., et al. 2018,
740 MNRAS, 481, 5098, doi: [10.1093/mnras/sty2573](https://doi.org/10.1093/mnras/sty2573)
- 741 Pasquato, M., & Milone, A. 2019, arXiv e-prints,
742 arXiv:1906.04983, doi: [10.48550/arXiv.1906.04983](https://doi.org/10.48550/arXiv.1906.04983)
- 743 Pedregosa, F., Varoquaux, G., Gramfort, A., et al. 2011,
744 Journal of Machine Learning Research, 12, 2825
- 745 Peebles, P. J. E., & Dicke, R. H. 1968, ApJ, 154, 891,
746 doi: [10.1086/149811](https://doi.org/10.1086/149811)
- 747 Peng, E. W., Ferguson, H. C., Goudfrooij, P., et al. 2011,
748 The Astrophysical Journal, 730, 23
- 749 Piotto, G. 2018, HST UV Globular Cluster Survey
750 ("HUGS"), STScI/MAST, doi: [10.17909/T9810F](https://doi.org/10.17909/T9810F)
- 751 Piotto, G., Bedin, L. R., Anderson, J., et al. 2007, The
752 Astrophysical Journal Letters, 661, L53,
753 doi: [10.1086/518503](https://doi.org/10.1086/518503)
- 754 Piotto, G., Milone, A. P., Bedin, L. R., et al. 2015, AJ, 149,
755 91, doi: [10.1088/0004-6256/149/3/91](https://doi.org/10.1088/0004-6256/149/3/91)
- 756 Plez, B. 2008, Physica Scripta Volume T, 133, 014003,
757 doi: [10.1088/0031-8949/2008/T133/014003](https://doi.org/10.1088/0031-8949/2008/T133/014003)
- 758 Prantzos, N., Charbonnel, C., & Iliadis, C. 2007, A&A, 470,
759 179, doi: [10.1051/0004-6361:20077205](https://doi.org/10.1051/0004-6361:20077205)
- 760 Renzini, A. 2008, Monthly Notices of the Royal
761 Astronomical Society, 391, 354,
762 doi: [10.1111/j.1365-2966.2008.13892.x](https://doi.org/10.1111/j.1365-2966.2008.13892.x)
- 763 Richer, H. B., Fahlman, G. G., Buonanno, R., et al. 1991,
764 ApJ, 381, 147, doi: [10.1086/170637](https://doi.org/10.1086/170637)
- 765 Rousseeuw, P. J. 1987, Journal of Computational and
766 Applied Mathematics, 20, 53,
767 doi: [https://doi.org/10.1016/0377-0427\(87\)90125-7](https://doi.org/10.1016/0377-0427(87)90125-7)
- 768 Salaris, M., & Cassisi, S. 2005, Evolution of stars and
769 stellar populations (John Wiley & Sons)
- 770 Sandage, A. R. 1953, AJ, 58, 61, doi: [10.1086/106822](https://doi.org/10.1086/106822)
- 771 Smith, G. H. 1987, Publications of the Astronomical
772 Society of the Pacific, 99, 67, doi: [10.1086/131958](https://doi.org/10.1086/131958)
- 773 Sneden, C., Kraft, R. P., Prosser, C. F., & Langer, G. 1992,
774 The Astronomical Journal, 104, 2121
- 775 Suntzeff, N. B., & Kraft, R. P. 1996, AJ, 111, 1913,
776 doi: [10.1086/117930](https://doi.org/10.1086/117930)
- 777 Valle, G., Dell'Omodarme, M., & Tognelli, E. 2022, A&A,
778 658, A141, doi: [10.1051/0004-6361/202142454](https://doi.org/10.1051/0004-6361/202142454)
- 779 van den Bergh, S. 2010, The Astronomical Journal, 140,
780 1043, doi: [10.1088/0004-6256/140/4/1043](https://doi.org/10.1088/0004-6256/140/4/1043)
- 781 Ventura, P., & D'Antona, F. 2009, A&A, 499, 835,
782 doi: [10.1051/0004-6361/200811139](https://doi.org/10.1051/0004-6361/200811139)
- 783 Ventura, P., D'Antona, F., Mazzitelli, I., & Gratton, R.
784 2001, ApJL, 550, L65, doi: [10.1086/319496](https://doi.org/10.1086/319496)